

Quick Fault-Plane Identification by a Geometrical Method: Application to the M_w 6.2 Leonidio Earthquake, 6 January 2008, Greece

J. Zahradnik and F. Gallovič

Charles University

E. Sokos, A. Serpetsidaki, and A. Tselentis

University of Patras

Online material: The hplot Matlab script, an aid for visualization of the *H-C* method of fault-plane identification.

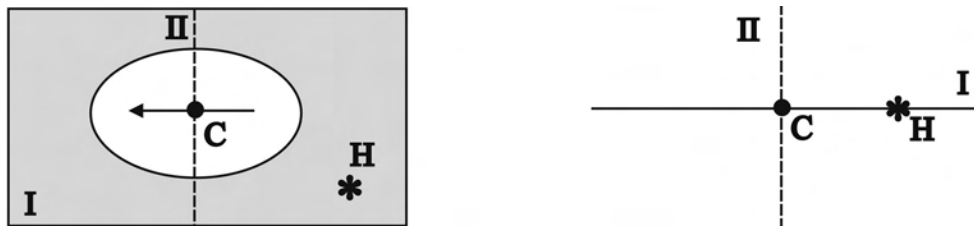
INTRODUCTION

Focal mechanisms of earthquakes provide two nodal planes. A foolproof method of identifying which one is the fault plane is the “seismologist’s dream.” This is true because knowledge of causative faults is of key importance for seismotectonic studies. For example, intermediate-depth earthquakes, such as the one studied in this paper, rarely have known fault planes, but the correct interpretation of such a fault plane would help constrain regional geodynamic models of subducted plates and stress fields. It is equally important to identify active crustal blind faults, knowledge of which may improve earthquake hazard assessment.

The fault plane can sometimes be well “mapped” (constrained) by the spatial distribution of numerous early aftershocks. However, this technique has serious limitations. One of them is the fact that in sparsely instrumented regions, accurate location of weak aftershocks is impossible. Moreover, some events lack numerous aftershocks at the mainshock fault plane altogether (this is typical of intermediate-depth earthquakes). The apparently straightforward case, where an earthquake occurs at or close to a geologically well-known fault, also benefits from an independent check, because the “known” fault may have a complex tectonic structure at depth.

The most challenging task is the *quick* identification of the earthquake fault plane. If made in near real time, it might play a vital role in the fast simulation of strong ground motions (shake maps) for post-event emergency services. If “quick” means a few hours or a few days after the event, the identification might still greatly contribute to assessing increased spatial probabilities of aftershocks based on the Coulomb stress-loading of neighboring faults due to the mainshock rupture (McCloskey *et al.* 2005).

Existing methods to identify the fault plane from seismograms are based mainly on finite-extent source models: distributed-slip models are generated for both nodal planes and the one that better fits the records is considered to be the fault plane. When near-fault records are available, this method can be applied even with very few stations (Delouis and Legrand 1999). However, using the nearest station records is highly vulnerable to location errors and complexities of the rupture process. Use of long-period regional or teleseismic records is also possible, often with relatively simple fault models. However, as a rule, the two nodal planes provide a waveform match that is just slightly different, so choosing one plane over the other often remains difficult (*e.g.*, Roumelioti *et al.* 2004). Conceptually similar are attempts to resolve the nodal-plane ambiguity by calculating the higher-order moment tensors for both planes and comparing the variance reduction; the advantage is that there is no need for a slip distribution model and applicability to weak events (McGuire 2004 and references therein). A new method to identify the fault by source scanning has recently been suggested by Kao and Shan (2007). In this method, the moment tensor solution is not needed, but other requirements are quite stringent, *e.g.*, the records must be close to the epicenter with well-separated *P* and *S* arrivals. Additional support of preferred slip directions on pre-existing zones of weakness can be also gained from the seismo-tectonic setting, in terms of regional stress fields and tractions acting on the nodal planes (Gephart 1985). In the case of well-expressed directivity effects, the macroseismic field may indicate the preferred nodal plane, even without any instrumental evidence. However, the macroseismic data are collected too late after the earthquake to provide a quick fault plane identification.



▲ **Figure 1.** Schematic explanation of the *H-C* method. Left: *H* (and star) = hypocenter, *C* = centroid, plane I and II are nodal planes, oval denotes a dominant slip region. Right: a different view of the same situation—a cross-section in which *H* identifies nodal plane I as the fault plane.



▲ **Figure 2.** Left: The typical situation, where *H* does not coincide exactly with any of the nodal planes. Right: Using several *H*s and *C*s, representing the uncertainty in their locations, can help to identify the fault plane.

THE *H-C* METHOD

This paper suggests a simple, innovative method, immediately applicable (under favorable conditions) when a reliable earthquake location and its centroid moment tensor solution (CMT) are available. Location, based on travel times, provides the hypocenter position (*H*), the place at which the rupture propagation initiated. The CMT solution from relatively long-period waveforms provides the centroid (*C*), which is the point-source approximation of the dominating slip region(s) on the fault. Further, the CMT solution also gives two planes passing through *C* (plane I and plane II) defined by the strike and dip angles of the moment-tensor solution.¹ Then, assuming a planar fault, the fault plane can be identified as that one among planes I and II that encompasses the hypocenter (Figure 1). In this paper this will be referred to as the *H-C* method. Although not yet broadly recognized as a useful tool for fault plane identification, its great potential is in simple linking of the independent pieces of short- and long-period seismic information.

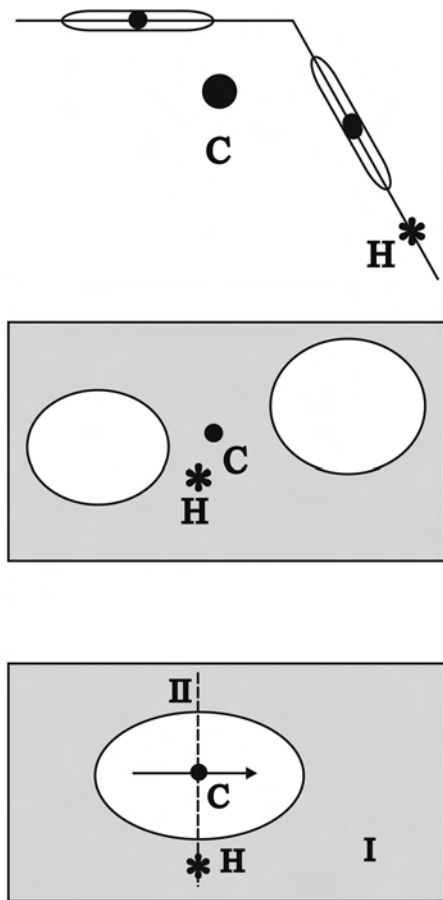
What are the favorable conditions under which the *H-C* method works? A successful application needs: 1) a reasonably accurate determination of the *H* and *C* position; 2) a sufficient distance between *H* and *C*, larger than the individual errors of the *H* and *C* positions; and 3) earthquake geometry that is not very complex (explained in more detail below). The orientation of planes I and II also plays a role, but their strike and dip angles are often stable enough during the MT inversion (say within 10° each). In this sense, the usual uncertainty of the fault plane solution is less critical than the *H* and *C* positions. For example, for earthquakes where the uncertainty of *H* and *C* is of the

1. For simplicity we may call them nodal planes, but, more often, this term is reserved for two planes passing through the hypocenter.

order of 10 km, the method becomes usable when the *H-C* distance gets larger than 10 km, *i.e.*, starting at about **M** 6. Under special conditions, for example, in the presence of a dense local network providing better constrained *H* and *C* parameters, the method might be applicable at about **M** 5. These are only rough estimates based on empirical relations between the fault size and magnitude (Somerville *et al.* 1999). In practice, it is also important whether the data “see” the whole fault (at very long periods) or the individual largest asperities, and whether the rupture nucleates in, close to, or far from the asperity (Mai *et al.* 2005).

Due to inherent uncertainties of the *H* and *C* positions, it is not possible to combine just any individual location with an individual CMT solution; more likely the hypocenter does not fall in any of the planes I and II (the so-called *H-C* inconsistency is detected, Figure 2 left). The correct approach is based on the concept of *collective* solutions (Figure 2 right). We seek families of acceptable solutions (a set of the hypocenter locations and a set of planes I or II given by inherent uncertainty, use of different methods, structural models, etc.), and compare them collectively. We arrive at the *H-C consistency* more often when considering uncertainties in this way.

Routine agency data typically provide the individual (rather than collective) solutions; *H* and *C* are often calculated by different teams. Therefore, the *H-C* method rarely works with very preliminary agency data. Or, at least, solutions of several agencies should be employed. Revised solutions may perform better, particularly if *S* waves from near stations are included for a better depth estimate, but a specific *H-C* study by a single team is always preferable. It can be performed quickly enough, especially if applied to previously studied geographic regions and using seismic networks with performance that is well known.



▲ **Figure 3.** Possible failures of the H - C method. Top: In this segmented fault, C , is out of both planar segments of the fault, including the segment encompassing H . Middle: In this almost symmetric bilateral rupture, although the fault is large, C appears too close to H when viewing the fault at very low frequencies. Bottom: the H - C line coincides with the intersection of plane I and II. H is in both nodal planes, so it cannot identify plane I as the fault plane.

Under such conditions, the operators are best aware of their alternative crustal models, the more and less reliable stations, noise levels, etc., so they can easily construct the families of the collective solutions, adequately reflecting typical model uncertainties due to varying data subsets.

A note regarding the C position: In practice, the MT inversion is often accompanied by a search of the source depth optimizing the waveform match, *i.e.*, assuming C under the epicenter. Although such an approximation may be good enough for retrieving the fault-plane solution, it is not sufficient for the H - C method. The C position should be searched in the 3D vicinity of the hypocenter and should extend sufficiently far, according to the magnitude of the studied earthquake (hence reflecting the expected fault length). We discuss this in more detail in the application section of this paper.

Last but not least, success of the H - C method is a matter of a suitable technique to *visualize* the geometrical configuration of the H , C , and planes I, II. We suggest a plotting tool allowing rotated (animated) 3D view (the `hcplot` script in Matlab, which

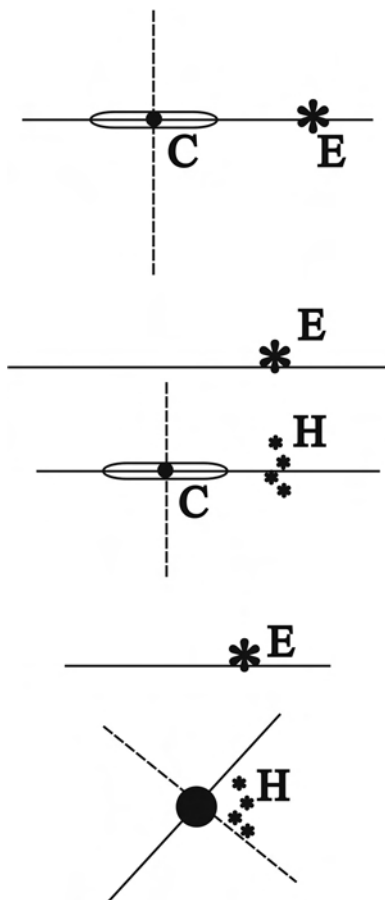
accompanies this paper in the electronic supplement). Note that we don't need to know the precise extent of the rupture to visualize planes I and II.

The price we pay for the simplicity and speed of the H - C method is in its limitations (Figure 3). First of all, we have to keep in mind that the method is nothing but a quick guess of the likely fault plane. There is no chance to validate the result within the method itself. Only independent, detailed (and thus not "quick") posterior studies can prove or disprove the fault-plane identification. There are also situations in which the H - C method can fail due not to inaccuracy in H and C , but for a more fundamental reason. Imagine a segmented, piecewise planar fault (Figure 3 top). If the CMT solution is calculated from low-frequency data, "seeing" all segments as a single point source, then C is out of both segments and neither of the planes I and II passing through C encompasses the hypocenter. A large non-DC component can signal the source complexity in cases like this (Frohlich 1994). Obviously, increasing frequency, so as to "see" the two asperities separately, can help to recognize at least the segment encompassing H . Even more difficult would be the case analogous to Figure 3, top panel, in which the segment containing H releases much less seismic moment than the other segment, thus apparently putting H out of the fault plane. At the low-frequency range, problems may arise even on a single fault when an almost symmetrical bilateral fault is represented by the centroid position C very near to H (Figure 3 middle). In such a case, it may help to consider the centroid time. Finally, let us mention that the H - C method always fails where the line connecting H and C coincides with the intersection of the planes I and II (Figure 3 bottom).

Obviously, the H - C method is not equally suited for all events of the same magnitude. It depends on the geometry of planes I and II with respect to the hypocenter, because the hypocenter depth is always more problematic than the epicenter position (E). Therefore, a strike-slip event with two vertical planes I and II is the easiest case to resolve successfully (Figure 4 top). The fault identification can be performed by means of the epicenter only, because the problematic depth has no effect. The map-view analysis is sufficient, so no 3D visualization is needed in this special case. A vertical dip-slip event (or low-dip thrust) is also easy (Figure 4 middle): The vertical plane, as a fault-plane candidate, can be simply accepted or rejected by means of the epicenter position only. Of course, to confirm the horizontal (or subhorizontal) plane, we already have to care more about the hypocenter depth. Oblique normal and reverse events are the most difficult ones (Figure 4 bottom): in case of a highly uncertain location depth, H may fall in both planes I and II.

TEST EXAMPLES

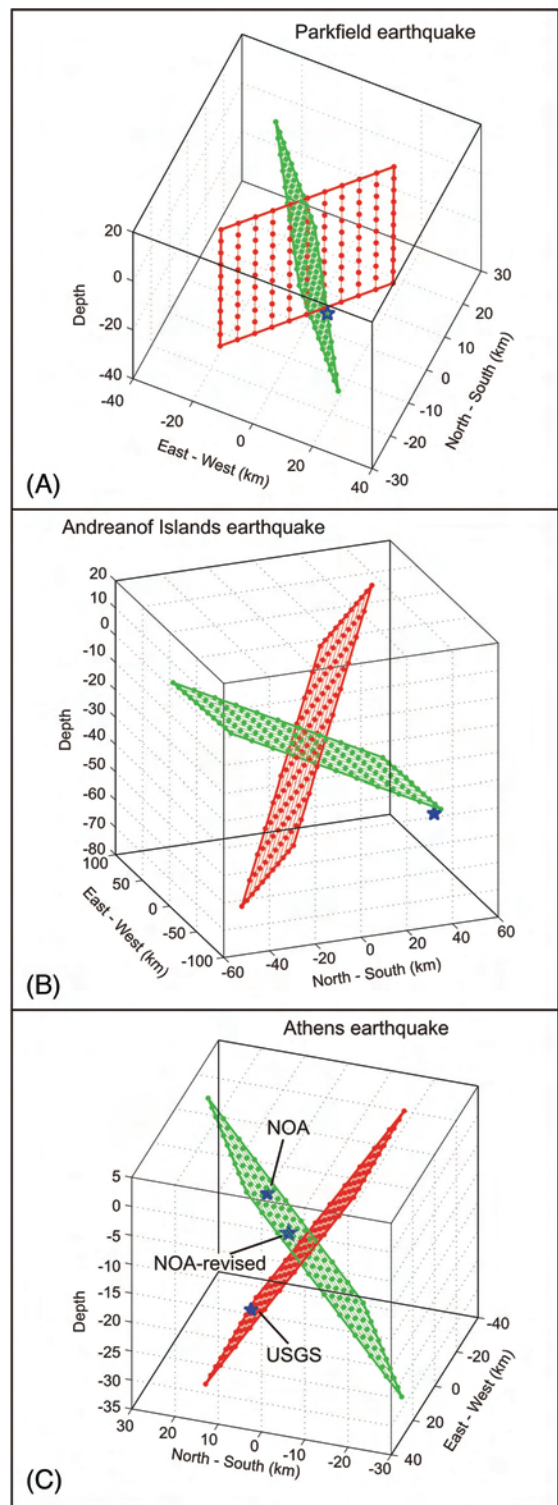
To demonstrate both easy and difficult cases, the H - C method is applied in this section to three earthquakes with known fault planes (Figure 5). For simplicity, only agency solutions are used, although generally they cannot be conclusive due to limited H - and C -position accuracy, as discussed above.



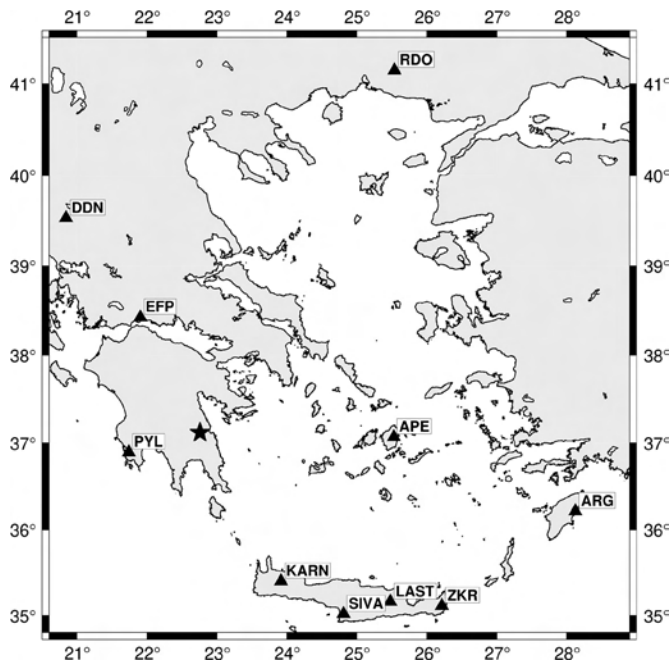
▲ **Figure 4.** A schematic illustration of the *H-C* method for different faulting mechanisms. Top: the simplest situation for a vertical strike slip when even a top view is helpful, without any 3D visualization, and epicenter *E* identifies the fault plane. Middle: a relatively easy fault plane identification for mechanisms when one of the nodal planes is vertical (or near vertical). Even *H* of inaccurate depth can successfully identify the fault plane. Bottom: The most difficult case of oblique fault planes. An *H* of inaccurate depth cannot solve this case, because it might appear equally close to both nodal planes.

Mw 6.0 Parkfield, Central California, 28 September 2004: The strike-slip case. Although based on the agency data (the Harvard CMT and the U.S. Geological Survey [USGS] location), the two individual solutions demonstrated that the hypocenter is closer to plane II, strike 321°, marked as green in Figure 5(A). This is the San Andreas fault segment, unambiguously mapped by the aftershock distribution (http://www.cisn.org/special/evt.04.09.28/Parkfield_DD/Park4.html; Thurber *et al.* 2006) and associated with the secondary surface rupture (Rymer *et al.* 2006).

Mw 7.1 Andreanof Islands, Aleutians, 19 December 2007: The low-angle thrust fault case. Even better than in the above example, the Harvard and USGS data are almost *H-C* consistent, and provide clear identification of the subhorizontal fault plane in Figure 5(B), typical of large subduction events in that region.



▲ **Figure 5.** Tests of the *H-C* method. (A) Parkfield, (B) Andreanof Islands, (C) Athens earthquake. Centroid is in the middle of the intersection of nodal planes I and II. Hypocenter is shown by the blue star. Only agency solutions are used: hypocenter of USGS and CMT of Harvard, except for the Athens earthquake. In the latter case two more hypocenter solutions are included (NOA preliminary and NOA revised). In all three tests the true fault plane is the green one, so the hypocenter should fall in that plane.



▲ **Figure 6.** Stations and networks (in brackets) used in the MT inversion: PYL, EFP, DDN [PSLNET, HP], ARG and RDO [GI-NOA, HL network], APE, LAST, ZKR, KARN, SIVA [GEOFON, GE].

M_w 6.0 Athens, Greece, 9 September 1999: The normal-fault case. This is an example of a difficult situation. As seen from Figure 5(C), the USGS location seems to prefer plane II (red, strike 284°) of the Harvard CMT solution, while the Greek Institute of Geodynamics, National Observatory of Athens (NOA) preliminary location identifies plane I (green, strike 116°). The NOA relocated hypocenter points to plane I again, which was indeed clearly mapped by the aftershock distribution as revealed by a temporary local network (Tselentis and Zahradnik 2000). In this case, using the individual agency solutions, the *H-C* method is not indicative enough. The reason is not only in the uncertainty of the solutions, but also in the less favorable geometry, as previously discussed (Figure 4 bottom).

The message of the test examples is simple: It is useful to try the *H-C* method even with preliminary agency data. If we get an *H-C* inconsistent case, it clearly shows that the *H* and *C* solutions need more accuracy. If we get an *H-C* consistent case, it still needs more verification. The next step is to add agency solutions, as they arrive after the earthquake, to obtain a more likely fault-plane candidate. Variability among the agency solutions also provides an uncertainty estimate, without which the *H-C* method cannot give reasonable results. Nevertheless, the most recommended procedure is a specifically focused application of the *H-C* concept, as illustrated in the next section.

M_w 6.2 LEONIDIO EARTHQUAKE

In this section, the *H-C* method introduced above is applied to the intermediate-depth earthquake of 6 January 2008 in southern Greece. The earthquake produced minor damage to

TABLE 1
Leonidio Earthquake; the Preferred Hypocenter Solution of this Paper. Crustal Model of Novotny *et al.* (2001), $V_p/V_s = 1.75$.

Origin (UTC)	Lat N (deg.)	Lon E (deg.)	Depth (km)
05:14:21	37.1055	22.7513	72

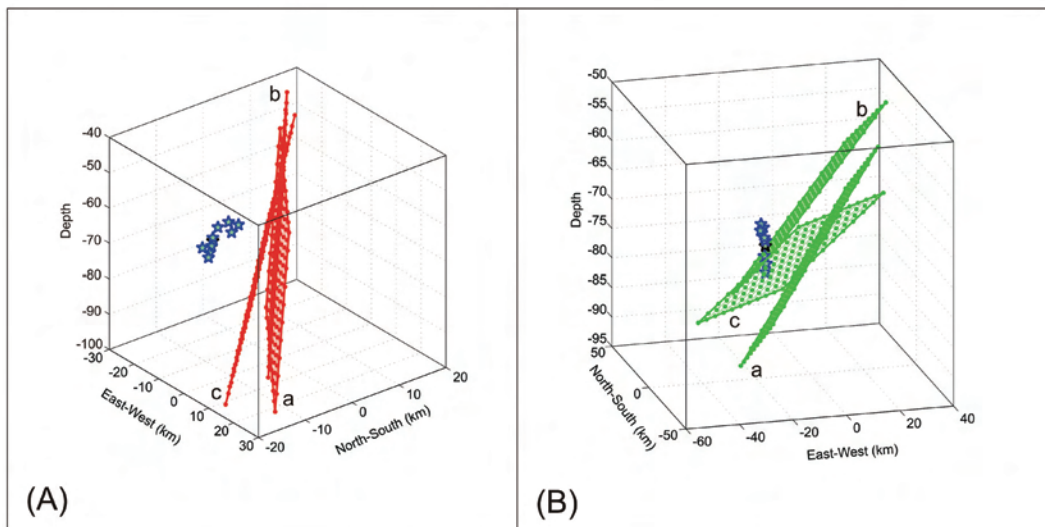
the city of Leonidio and the surrounding region on the eastern coast of the Peloponnese, 120 km from Athens, but it was felt all over the country and in several places in southern Italy. Only a few aftershocks were located by regional networks: four $M_L \sim 3$ events and one $M 4$ event as late as 11 January; these definitely could not map the fault plane.

Hypocenter location. The HYPOINVERSE code was applied to invert the manual *P* and *S* picks from 15 stations; those used below for CMT (Figure 6), plus some extra stations (short period) from the Patras Seismological Laboratory network (PSLNET) and a few stations belonging to Aristotle University of Thessaloniki, up to 350 km away. The uncertainty was evaluated by repeated calculations with: a) various starting depths; b) various data subsets, *e.g.*, keeping only stations closer than 200 km; c) two V_p/V_s ratios; and d) two crustal models (Tselentis *et al.* 1996; Novotny *et al.* 2001). The latter provided the least root mean square (RMS) residuals, in particular for $V_p/V_s = 1.75$. The best-fitting location is shown in Table 1. The family of alternative hypocenter solutions is plotted in Figures 7 and 8.

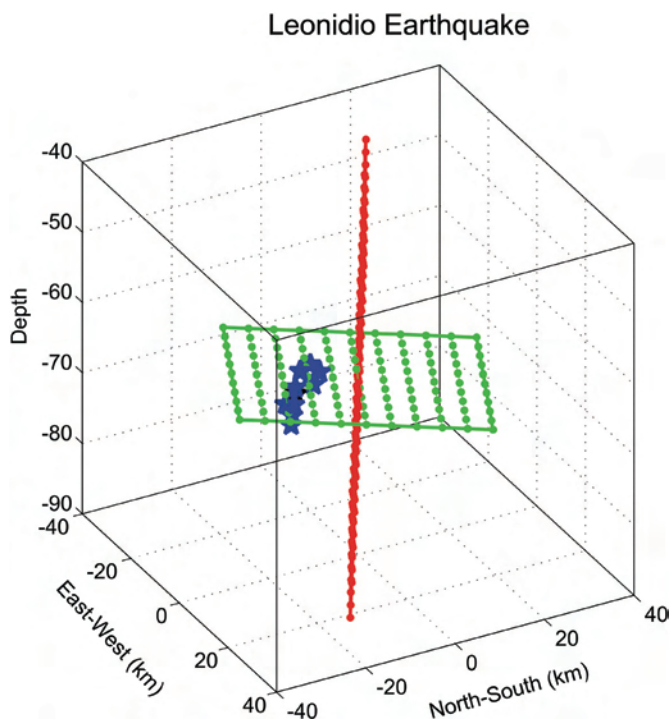
CMT solution. Broadband records from the permanent seismological network PSLNET were studied, complemented with waveforms provided by other near-regional stations available through the ORFEUS data center and the GEOFON network. Finally, three-component unclipped records from 10 stations were used in the MT inversion, providing fairly good azimuthal coverage of the event (Figure 6). Furthermore, the EW horizontal component (clipped) of the nearest station, PYL, was excluded. The epicentral distances range from 117 km to 490 km.

Various preliminary tests were carried out to find the appropriate crustal model and frequency band to achieve an acceptable waveform match. In particular, the crustal models proposed by Endrun *et al.* (2004) and Novotny *et al.* (2001) were tested at frequencies below 0.1 Hz. Finally, all the runs were performed in the model of Novotny *et al.* (2001), which provided a slightly better match,² using displacement waveforms from 0.02 to 0.07 Hz. The MT calculations were made with ISOLA software, available at <http://seismo.geology.upatras.gr/isola> (Sokos and Zahradnik 2008). Final runs included the centroid grid search in a 7×7 horizontal stencil (step 7 km) at three depths (step 5 km). The whole procedure was performed several times, with or without the *Z* and *NS* components of the PYL

2. In this paper, the model of Novotny *et al.* (2001) occasionally proved to be good for location as well as the MT inversion. However, in general, use of a single crustal model for both tasks is not necessary; the existing crustal models are rarely equally suitable in both the short- and long-period range.



▲ **Figure 7.** Application of the *H-C* method to the Leonidio earthquake. (A) Three high-dip nodal planes illustrating uncertainty of the centroid determination. Centroid is in the middle of each plane. The blue stars show the family of hypocenter solutions of this paper. With such a distance between the hypocenters and the planes, it is unlikely that the high-dip nodal plane was the fault plane. (B) As in (A), but for the corresponding low-dip nodal planes. Proximity of the hypocenters (stars) to the planes indicates that the earthquake ruptured along such a low-dip fault. The three CMT solutions are as follows: (a) without station PYL, (b) with PYL-Z; (c) with PYL-Z and PYL-N.



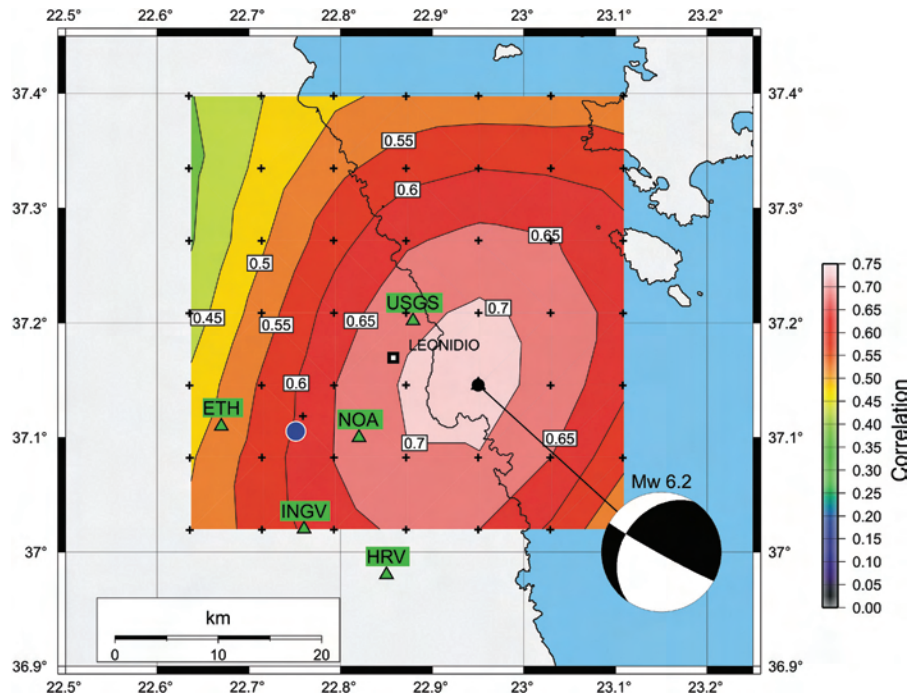
▲ **Figure 8.** The *H-C* plot of the preferred solution (Tables 1 and 2). Nodal planes I and II are shown in red and green, respectively. Centroid is in the middle of the intersection of the nodal planes. The alternative hypocenter solutions of the mainshock are shown in blue. The green plane encompasses the hypocenters, thus this low-dip nodal plane (strike 213°, dip 34°) is identified as the likely fault plane.

Centroid Time (UTC)	Lat N (deg.)	Lon E (deg.)	Depth (km)	Scalar moment (Nm)	M_w
05:14:25	37.1457	22.9502	65	1.5e+18	6.2
Strike I	Dip I	Rake I	Strike II	Dip II	Rake II
119°	87°	124°	213°	34°	5°
P-axis	Trend	Plunge	T-axis	Trend	Plunge
	181°	34°		59°	38°

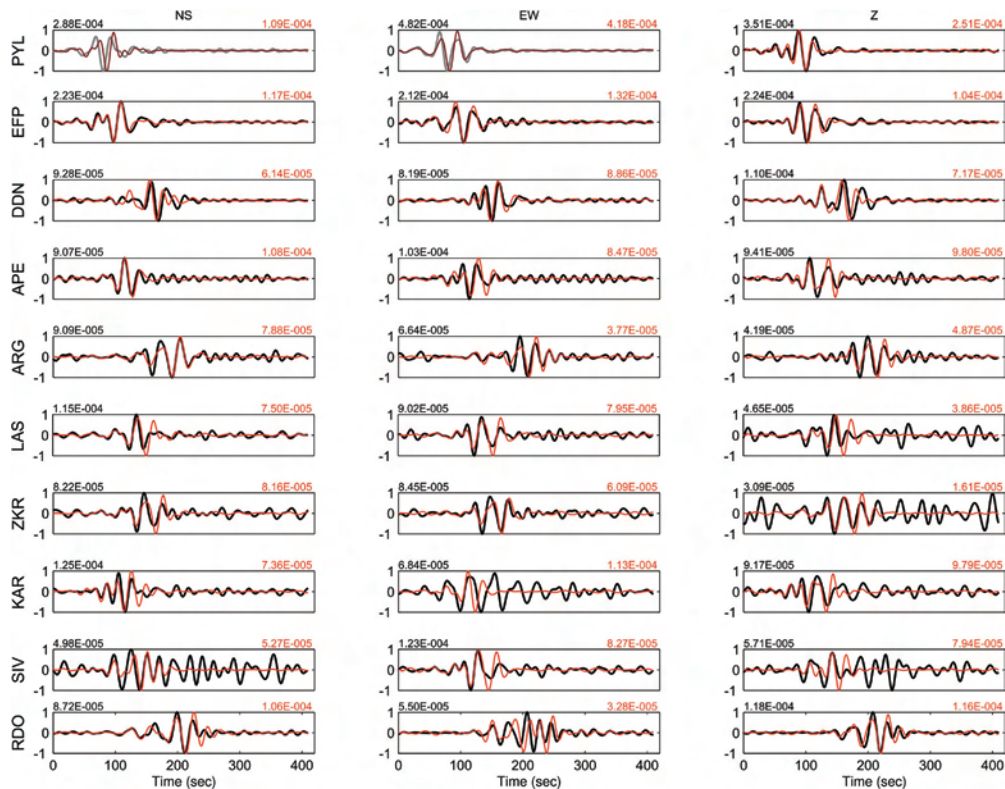
station. Stability of the MT solution (the *C* position and the corresponding strike, dip, rake) was proved by jackknifing, *i.e.*, by repeatedly removing one station. The inversions indicate the NS position of *C* to be the most stable, the EW position plus/minus one 7-km grid step, and the *C* depth the least resolved, between 60 and 80 km. The preferred solution, considering the waveform match and the *H-C* consistency, is shown in Table 2 (the solution with the PYL-Z component). Three samples of the family of the alternative solutions are plotted in Figure 7.

*The H-C analysis.*³ The nodal planes of the Leonidio earthquake differ considerably in their dip: plane I is almost vertical (strike of about 120°), and plane II has a low dip ~ 35° (strike of about 210°). Accordingly to our method section, this is a favorable situation. Figure 7 compares the position of the nodal planes

3. A quick preliminary result (Zahradnik *et al.* 2008a) was posted on the Web page of the European-Mediterranean Seismological Centre within one week of the earthquake.



▲ **Figure 9.** Map view of correlation between the observed and synthetic waveforms at the depth of 65 km for the preferred solution. The preferred epicenter solution of this paper (Table 1) is shown by blue circle. Small black crosses mark the trial source positions at which the MT solution was performed, at various depths. The preferred centroid position (Table 3), the black dot, is connected with the corresponding “beach ball.” The maximum correlation value 0.72 corresponds to the overall variance reduction of 0.51 at 10 stations. For comparison, the centroid positions of several agencies are shown by green triangles.



▲ **Figure 10.** Waveform match between the observed (black) and synthetic (red) waveforms for the preferred CMT solution. Maximum amplitudes are shown at the top of each panel in the same color. Gray waveforms weren’t used in the inversion.

and the hypocenter solutions, separately for the high- and low-dip planes. Without a doubt, the hypocenter matches much better with the low-dip nodal plane. The preferred *H-C* solution is presented in Figure 8; the hypocenter of Table 2 is 2 km from the low-dip plane and 13 km from the high-dip one. (The animated 3D version of the plot [leonidio.avi] is in the electronic supplement.) Figure 9 gives the map view of the solution, together with the spatial correlation between the observed and synthetic waveforms. Finally, in Figure 10 a fairly reasonable waveform match between synthetic and observed waveforms is documented; the overall variance reduction is 0.51.

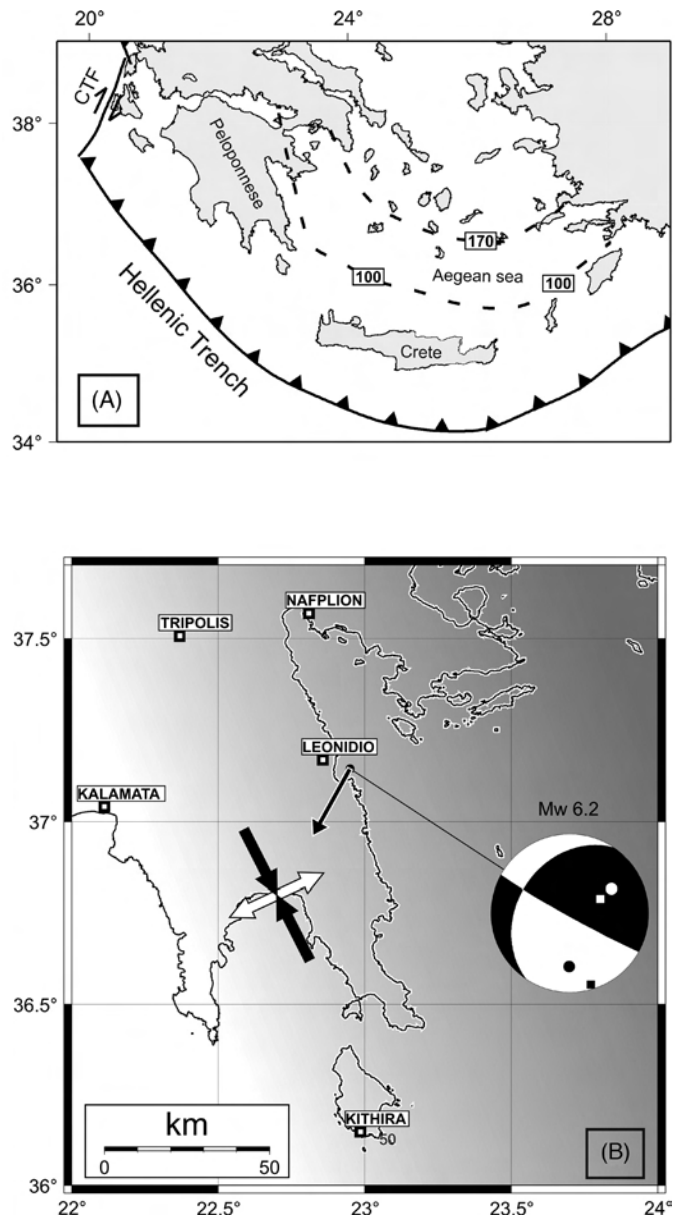
A few remarks to complement the analysis follow:

All tests provided an almost double-couple event, with a surprisingly stable and high DC percentage (around 90%). In contrast to complex events accompanied by low DC% (Zahradnik *et al.* 2008b), the Leonidio earthquake seems to represent a relatively simple rupture. The independent preliminary analysis shows that teleseismic data are in agreement with this observation (Kiratzi and Benetatos 2008).

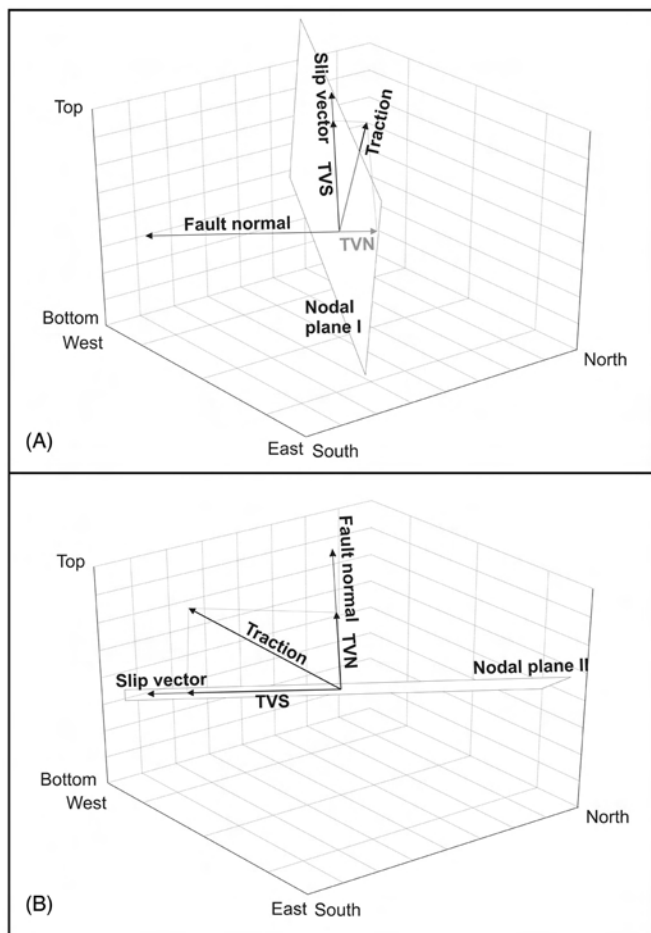
Regarding the MT solutions of the other agencies, this paper is closer to the USGS CMT solution.

The significant difference between the centroid and origin time (of about 4 seconds), reported also by USGS, Harvard, and the Italian Istituto Nazionale di Geofisica e Vulcanologia (INGV) is another very stable feature of this event.

Tectonics and stress field. Finally we discuss the preferred solution in the frame of the seismotectonic environment. Since the Leonidio earthquake was not preceded by any earthquake that could be considered an obvious triggering event, it had to be invoked predominantly by the regional stress. The regional stress tensor in the studied region was investigated by Kiratzi and Papazachos (1995). The authors used five MT solutions of earthquakes $M_s > 5$ in the western part of the Hellenic arc (their region 1A). The strain-rate orientations associated with their stress tensor implied that the tectonic setting is characterized by a shortening of the subducting plate in a direction parallel to the trend of the Hellenic arc, basically in agreement with independent GPS data and geodynamic models. The regional stress is characterized by the dominant tension (azimuth 65° , plunge 55°), roughly perpendicular to the strike of the Hellenic arc in the studied region, and the subhorizontal pressure (azimuth 163° , plunge 6°) pointing along the arc (Figure 11). Furthermore, we found that the principal directions of this regional stress correspond to the smallest mean rotation angles (Kagan 1991) with respect to the *P* and *T* axes of the earthquake moment tensors involved in the stress inversion. Using the regional stress tensor (of unknown absolute value, thus normalized to unity), we evaluate the dimensionless traction for both nodal planes I and II of the Leonidio earthquake. We let TVN be the normal component of the traction vector with respect to the nodal plane and TVS the tangential component of the traction parallel to the slip vector, all calculated separately for both nodal planes (Figure 12 and Table 3). The normal components differ substantially for planes I and II. While the TVN is negative for plane I, it is positive for plane II. Therefore, the Coulomb failure



▲ **Figure 11.** Tectonics and stress field in the studied region. (A) Hellenic trench, Greece, where the African plate is subducting below the Aegean plate. CTF is the Cefallonia transform fault. Isolines in the Aegean Sea are mean depths of earthquakes (after Papazachos *et al.* 2000). (B) The increasing gray shade is a schematic illustration of the increasing depth of slab in the region (after Gudmundsson and Sambridge 1998). The *P* and *T* axes of the regional stress field (Kiratzi and Papazachos 1995), projected onto the horizontal plane, are shown by the arrows (the true *T/P* eigenvalue ratio is 1.25). The beach ball for the Leonidio earthquake, connected with the centroid, shows the *P* and *T* axes of the earthquake in circles, while those of the regional field are marked by squares. The main result of this paper, *i.e.*, the identification of the fault plane, is represented by the slip vector of the studied event (strike 209° , dip 3°). It shows the almost strike-slip motion of the top (hanging) block, as it moves along the low-dipping fault plane inferred in this paper.



▲ **Figure 12.** Computed tractions corresponding to the regional stress field acting on the two nodal planes (I and II) of the Leonidio earthquake. TVS = the tangential component of the traction parallel to the slip vector, TVN = the normal component of the traction vector (Table 3). Note that the TVN value differs for planes I and II: while for plane II it is positive, for plane I it is negative. In this sense the Coulomb failure model supports the findings of the *H-C* method that the Leonidio earthquake ruptured the low-dip nodal plane II.

function $CFF = TVS + \mu TVN$ also differs for the two slip vectors: $CFF = 0.70$ for the slip vector in the high-dip plane I, and $CFF = 1.07$ for the low-dip plane II. Here the effective friction coefficient $\mu = 0.5$ is used. Generally, for deeper earthquakes, a higher value is also possible (Tibi *et al.* 2003), say $\mu = 0.8$, thus further increasing the difference between planes I and II. If assuming a preexisting zone of weakness, the larger value of the stress criterion is an independent indication supporting plane II as the fault plane. Considering this together with the results of the *H-C* method discussed above, we conclude that the Leonidio earthquake ruptured along the low-dip plane II.

CONCLUSION

It is important to develop new methods for quick identification of an earthquake fault plane, without having to wait for the

TABLE 3
Leonidio Earthquake and Its Interaction with the Regional (Unit) Stress Tensor: TVS = the Tangential Component of the Traction Parallel to the Slip Vector, TVN = the Normal Component of the Traction with Respect to the Nodal Plane, CFF = the Coulomb Failure Function; All Values Dimensionless.

Nodal plane	TVS	TVN	CFF
I	0.7941	-0.1962	0.6960
II	0.7906	0.5522	1.0667

occurrence of aftershocks (if any, and if located satisfactorily). In particular, we need new methods that can be applied sooner than more complex and time-demanding studies, such as slip inversions, source-scanning algorithms, etc. The *H-C* method introduced in this paper allows identification of the fault plane by analyzing the geometrical configuration of the hypocenter (*H*), centroid (*C*), and the moment-tensor solution (nodal planes I and II). Note that such a successful though simple approach has not yet been recognized.

We applied this method to the Leonidio earthquake of 6 January 2008. Taking into account uncertainties of the location and the waveform inversion, the near-regional waveform data from 117 km to 490 km, at frequencies 0.02 to 0.07 Hz, suggested that the *M_w* 6.2 Leonidio earthquake, along the eastern coast of the Peloponnese, represented *strike-slip motion along the low-dip fault plane* (strike 213°, dip 34°, rake 5°). Based on the regional stress field (Kiratzi and Papazachos 1995), characterized by shortening of the subducting plate in a direction parallel to the trend of the Hellenic arc, this preference for the low-dip plane was also supported by a quantitative estimate of the Coulomb failure function. As there were not enough Leonidio earthquake aftershocks to enable identification of the fault plane by the usual methods, the *H-C* method might be valuable for studies of the subduction process. In general, the *H-C* method may be useful in early warning systems and emergency operations after catastrophic events.

During the writing of this paper, the *H-C* method was applied to two more earthquakes in southern Greece, an *M* 6.9 on 14 February 2008 and an *M* 6.2, on 20 February 2008, and in each case preliminary identification of the fault plane was quickly (within one day) reported to the European-Mediterranean Seismological Centre (EMSC). These preliminary assessments can be found at <http://www.emsc-csem.org/index.php?page=current&sub=recent>.

To encourage a broader use of the *H-C* method, a visualization tool (the *hcplot* Matlab script) accompanies this paper in the form of an electronic supplement. The script quickly produces a 3D animated plot of the hypocenter, centroid, and nodal planes. The code is self-explanatory, intuitive, and easy-to-use. It is also possible to produce a movie for presentation purposes, independently of the Matlab environment. The electronic supplement includes a movie (*leonidio.avi*) related to the 6 January 2008 Leonidio earthquake. ☒

ACKNOWLEDGMENTS

The authors acknowledge free access to waveforms of various European networks (MEDNET, GEOFON, GI-NOA) through ORFEUS and GEOFON data centers. The use of phase data from stations belonging to Aristotle University of Thessaloniki is also acknowledged. The work is a part of the following projects supported in the Czech Republic: GACR 205/07/0502, PostDoc GACR 205/08/P013, GAUK 279/2006/B-GEO/MFF, MSM 0021620860.

REFERENCES

- Delouis, B., and D. Legrand (1999). Focal mechanism determination and identification of the fault plane of earthquakes using only one or two near-source seismic recordings. *Bulletin of the Seismological Society of America* **89**, 1,558–1,574.
- Endrun, B., T. Meier, M. Bischoff, and H.-P. Harjes (2004). Lithospheric structure in the area of Crete constrained by receiver functions and dispersion analysis of Rayleigh phase velocities. *Geophysical Journal International* **158**, 592–608.
- Frohlich, C. (1994). Earthquakes with non-double-couple mechanisms. *Science* **264**, 804–809.
- Gephart, J. W. (1985). Principal stress directions and the ambiguity in fault plane identification from focal mechanisms. *Bulletin of the Seismological Society of America* **75**, 621–625.
- Gudmundsson, O., and M. Sambridge (1998). A regionalized upper mantle (RUM) seismic model. *Journal of Geophysical Research* **B4**, 7,121–7,136.
- Kagan, Y.Y. (1991). 3-D rotation of double-couple earthquake sources. *Geophysical Journal International* **106**, 709–716.
- Kao, H., and S.-J. Shan (2007). Rapid identification of earthquake rupture plane using Source-Scanning Algorithm. *Geophysical Journal International* **168**, 1,011–1,020.
- Kiratzí, A. A., and C. B. Papazachos (1995). Active seismic deformation in the southern Aegean Benioff zone. *Journal of Geodynamics* **19**, 65–78.
- Kiratzí, A., and Ch. Benetatos (2008). The 6 January 2008 (*M_w* 6.2) Leonidio (southern Greece) intermediate depth earthquake: Teleseismic body wave modeling. Report to EMSC Web page, <http://www.emsc-csem.org/index.php?page=current&sub=recent>.
- Mai, P. M., P. Spudich, and J. Boatwright (2005). Hypocenter locations in finite-source rupture models. *Bulletin of the Seismological Society of America* **95**, 965–980.
- McCloskey, J., S. S. Nalbant, and S. Steacy (2005). Earthquake risk from co-seismic stress. *Nature* **434**, 291.
- McGuire, J. J. (2004). Estimating finite source properties of small earthquake ruptures. *Bulletin of the Seismological Society of America* **94**, 377–393.
- Novotny, O., J. Zahradnik, and G.-A. Tselentis (2001). Northwestern Turkey earthquakes and the crustal structure inferred from surface waves observed in the Corinth Gulf, Greece. *Bulletin of the Seismological Society of America* **91**, 875–879.
- Papazachos, B. C., V. G. Karakostas, C. B. Papazachos, and E. M. Scordilis (2000). The geometry of the Wadati-Benioff zone and lithospheric kinematics in the Hellenic arc. *Tectonophysics* **319**, 275–300.
- Roumelioti, Z., Ch. Benetatos, A. Kiratzí, G. Stavrakakis, and N. Melis (2004). A study of the 2 December 2002 (*M* 5.5) Vartholomio (western Peloponnese, Greece) earthquake and of its largest aftershocks. *Tectonophysics* **387**, 65–79.
- Rymer, M. J., J. C. Tinsley III, J. A. Treiman, J. R. Arrowsmith, K. B. Clahan, A. M. Rossinski, W. A. Bryant, H. A. Snyder, G. S. Fuis, N. A. Toke, and G. W. Bawden (2006). Surface fault slip associated with the 2004 Parkfield, California, earthquake. *Bulletin of the Seismological Society of America* **91**, 211–220.
- Sokos, E., and J. Zahradnik (2008). ISOLA a Fortran code and a Matlab GUI to perform multiple-point source inversion of seismic data, *Computers & Geosciences* **34** (8), 967–977.
- Somerville, P., K. Irikura, R. Graves, S. Sawada, D. Wald, N. Abrahamson, Y. Iwasaki, T. Kagawa, N. Smith, and A. Kowada (1999). Characterizing crustal earthquake slip models for the prediction of strong ground motion. *Seismological Research Letters* **70**, 59–80.
- Thurber, C., H. Zhang, F. Waldhauser, J. Hardebeck, A. Michael, and D. Eberhart-Phillips (2006). Three-dimensional compressional wavespeed model, earthquake relocations, and focal mechanisms for the Parkfield, California, region. *Bulletin of the Seismological Society of America* **96**, S38–S49.
- Tibi, R., D. A. Wiens, and H. Inoue (2003). Remote triggering of deep earthquakes in the 2002 Tonga sequences. *Nature* **424**, 921–925.
- Tselentis, G.-A., N. S. Melis, E. Sokos, and K. Papatsimpa (1996). The Egeion June 15, 1995 (6.2 ML) earthquake, western Greece. *Pure and Applied Geophysics* **147**, 83–98.
- Tselentis, G.-A., and J. Zahradnik (2000). Aftershock monitoring of the Athens earthquake of September 7, 1999. *Seismological Research Letters* **71**, 330–337.
- Zahradnik, J., E. Sokos, A. Serpetsidaki, and G.-A. Tselentis (2008a). The *M_w* 6.2 Leonidio, southern Greece earthquake of January 6, 2008: Preliminary identification of the fault plane. Report to EMSC Web page, <http://www.emsc-csem.org/index.php?page=current&sub=recent>.
- Zahradnik, J., E. Sokos, G.-A. Tselentis, and N. Martakis (2008b). Non-double-couple mechanism of moderate earthquakes near Zakynthos, Greece, April 2006: Explanation in terms of complexity. *Geophysical Prospecting* **56**, 341–356.

*University of Patras Geology Department
Seismological Laboratory
Rio 26504, Patras, Greece
esokos@upatras.gr
(E.S.)*